MARTIN MARIETTA ENERGY SYSTEMS LIBRARIES
3 4456 0064725 4

ORNL/TM-10034

ornl

OAK RIDGE
NATIONAL
LABORATORY

MARTIN MARIETTA

Vectorized Difference Schemes for a Three Dimensional Enthalpy Formulation for Phase Change Problems

M. A. Williams
D. G. Wilson

OPERATED BY
MARTIN MARIETTA ENERGY SYSTEMS, INC.
FOR THE UNITED STATES
DEPARTMENT OF ENERGY

Printed in the United States of America. Available from
National Technical Information Service
U.S. Department of Commerce
5285 Port Royal Road, Springfield, Virginia 22161
NTIS price codes—Printed Copy: A03; Microfiche A01

This report was prepared as an account of work sponsored by an agency of the United States Government. Neither the United States Government nor any agency thereof, nor any of their employees, makes any warranty, express or implied, or assumes any legal liability or responsibility for the accuracy, completeness, or usefulness of any information, apparatus, product, or process disclosed, or represents that its use would not infringe privately owned rights. Reference herein to any specific commercial product, process, or service by trade name, trademark, manufacturer, or otherwise, does not necessarily constitute or imply its endorsement, recommendation, or favoring by the United States Government or any agency thereof. The views and opinions of authors expressed herein do not necessarily state or reflect those of the United States Government or any agency thereof.

ORNL/TM-10034

Engineering Physics and Mathematics Division
Mathematical Sciences Section

VECTORIZED DIFFERENCE SCHEMES FOR A THREE DIMENSIONAL ENTHALPY FORMULATION FOR PHASE CHANGE PROBLEMS

M. A. Williams

Engineering Physics and Mathematics Division
Oak Ridge National Laboratory
Oak Ridge, Tennessee 37831
and
Mathematics Department
Lehigh University
Bethlehem, PA 18015

D. G. Wilson

Engineering Physics and Mathematics Division
Oak Ridge National Laboratory
Oak Ridge, Tennessee 37831

Date Published: July 1986

Research sponsored by the
Applied Mathematical Sciences Research Program
U.S. Department of Energy
Office of Energy Research

Prepared by the
Oak Ridge National Laboratory
Oak Ridge, Tennessee 37831
operated by
Martin Marietta Energy Systems, Inc.
for the
U.S. DEPARTMENT OF ENERGY
under Contract No. DE-AC05-84OR21400

MARTIN MARIETTA ENERGY SYSTEMS LIBRARIES
3 4456 0064725 4

CONTENTS

Abstract 1

1. Introduction 1

2. Enthalpy Formulation 2

3. Numerical Formulation 3

4. Numerical Solution 7

5. CRAY X-MP Implementation 9

6. Test Results 15

References 18

VECTORIZED DIFFERENCE SCHEMES FOR A THREE DIMENSIONAL ENTHALPY FORMULATION FOR PHASE CHANGE PROBLEMS

M. A. Williams
D. G. Wilson

ABSTRACT

Fully vectorized codes have been written for the CRAY X-MP implementing explicit and implicit finite difference schemes for enthalpy formulations of three dimensional Stefan-like problems. The implicit scheme is that proposed by C. M. Elliot and J. R. Ockendon. The explicit scheme is intended to provide a comparison for the results from the implicit scheme. Vectorization of the code required some ingenuity since material properties change discontinuously as solidification proceeds. Boolean variables were used to avoid conditional branches in DO loops. Average vector length was greatly increased by unfolding three dimensional arrays and treating them as long vectors. This report documents the development of the code and the vectorization strategies. The investigation of the tradeoffs between the implicit scheme, potentially capable of taking large time steps, and the explicit scheme, whose time step size is limited by the stability criterion, has begun but is not complete.

1. Introduction

Numerical methods for Stefan problems are based on discretization of either the heat equation or the equations of the enthalpy formulation. Crank [1] and Elliott and Ockendon [2] survey a number of these techniques. In this paper we present an algorithm suggested by Elliott and Ockendon [2] and its implementation on the CRAY X-MP. The algorithm admits both explicit and implicit finite difference implementations. Explicit solutions can be calculated quickly at each time increment but stability considerations restrict the time step size. Alternatively, implicit schemes are unconditionally stable and thus the time step size is not restricted, but an iterative method must be used to solve the

non-linear system at each time level. We have developed a computer code to be used in investigating trade offs between these methods.

We consider the problem of solidifying a three dimensional rectangular parallelepiped of material initially at its critical temperature. The boundary conditions imposed are the temperature distribution on the bottom of the box and zero flux on the walls and top of the box. We first present an enthalpy formulation of a moving boundary problem and the corresponding numerical formulation. Next, we discuss the method suggested by Elliott and Ockendon [2] in which self-consistent enthalpy and temperature values are calculated at each node using Gauss-Seidel iterations and successive overrelaxation (SOR) to solve the non-linear system. In Section 5, implementation considerations for the CRAY X-MP are discussed. Red/black ordering of nodes is introduced to eliminate vectorization problems created by Gauss-Seidel iteration. Boolean variables are introduced to avoid IF statements within loops since IF statements inhibit vectorization. Finally, results of numerical experiments and graphical output are presented.

2. Enthalpy Formulation

The enthalpy formulation of the two-phase Stefan problem consists of two relations to be solved simultaneously. The first is given by

$$e = \begin{cases} \int_{T_{cr}}^{T} c(\tau)\, d\tau & T < T_{cr} \\ 0 < e < H & T = T_{cr} \\ \int_{T_{cr}}^{T} c(\tau)\, d\tau + H & T > T_{cr} \end{cases}$$

Here e is enthalpy, T temperature, T_{cr} the critical temperature, c the heat capacity, and H the latent heat. Here e is not given as a function of T. There is an inclusion when $T = T_{cr}$. Alternately, the enthalpy/temperature relationship may be written

$$T = \begin{cases} T_{cr} - \int_e^0 \frac{d\zeta}{c(\zeta)} & e \leqslant 0 \\ T_{cr} & 0 < e < H \\ T_{cr} + \int_H^e \frac{d\zeta}{c(\zeta)} & e \geqslant H \end{cases} ,$$

where now temperature is a function of enthalpy. If the heat capacities are constant in the solid and liquid, these relations reduce to

$$e = \begin{cases} c_S (T - T_{cr}) & T < T_{cr} \\ 0 < e < H & T = T_{cr} \\ c_L (T - T_{cr}) + H & T > T_{cr} \end{cases}$$

and

$$T = \begin{cases} T_{cr} + e/c_S & e \leqslant 0 \\ T_{cr} & 0 < e < H \\ T_{cr} + (e - H)/c_L & e \geqslant H \end{cases}$$

where c_S and c_L are the specific heats of the solid and liquid respectively. See Figure 1. The second relation to be solved is an equation relating changes in enthalpy to temperature gradients and is given by

$$\rho e_t = div(k(T) grad T) ,$$

where $k(T)$ is the thermal conductivity, and ρ is the constant density. This can be expressed in cartesian coordinates as

$$\rho e_t = (k(T)T_x)_x + (k(T)T_y)_y + (k(T)T_z)_z . \tag{1}$$

3. Numerical Formulation

Consider partitioning the rectangular parallelepiped $[0, lx] \times [0, ly] \times [0, lz]$. First, consider the intervals $0 < x < lx$ and $0 < y < ly$. Given positive integers nx and ny, set $\Delta x = lx/nx$ and $\Delta y = ly/ny$. We require that nx and ny be odd for reasons explained in Section 5. We partition the intervals $[0, lx]$ and $[0, ly]$ as follows. Let $x_j = j\,\Delta x$ for $j = 0, 1, 2, \ldots, nx$ and $y_j = j\,\Delta x$ for $j = 0, 1, 2, \ldots, ny$. Denote by I_j the interval (x_{j-1}, x_j) for $j = 1, 2, \ldots, nx$ and by J_j the interval (y_{j-1}, y_j) for $j = 1, 2, \ldots, ny$. The I

ORNL-DWG 81-17655RA

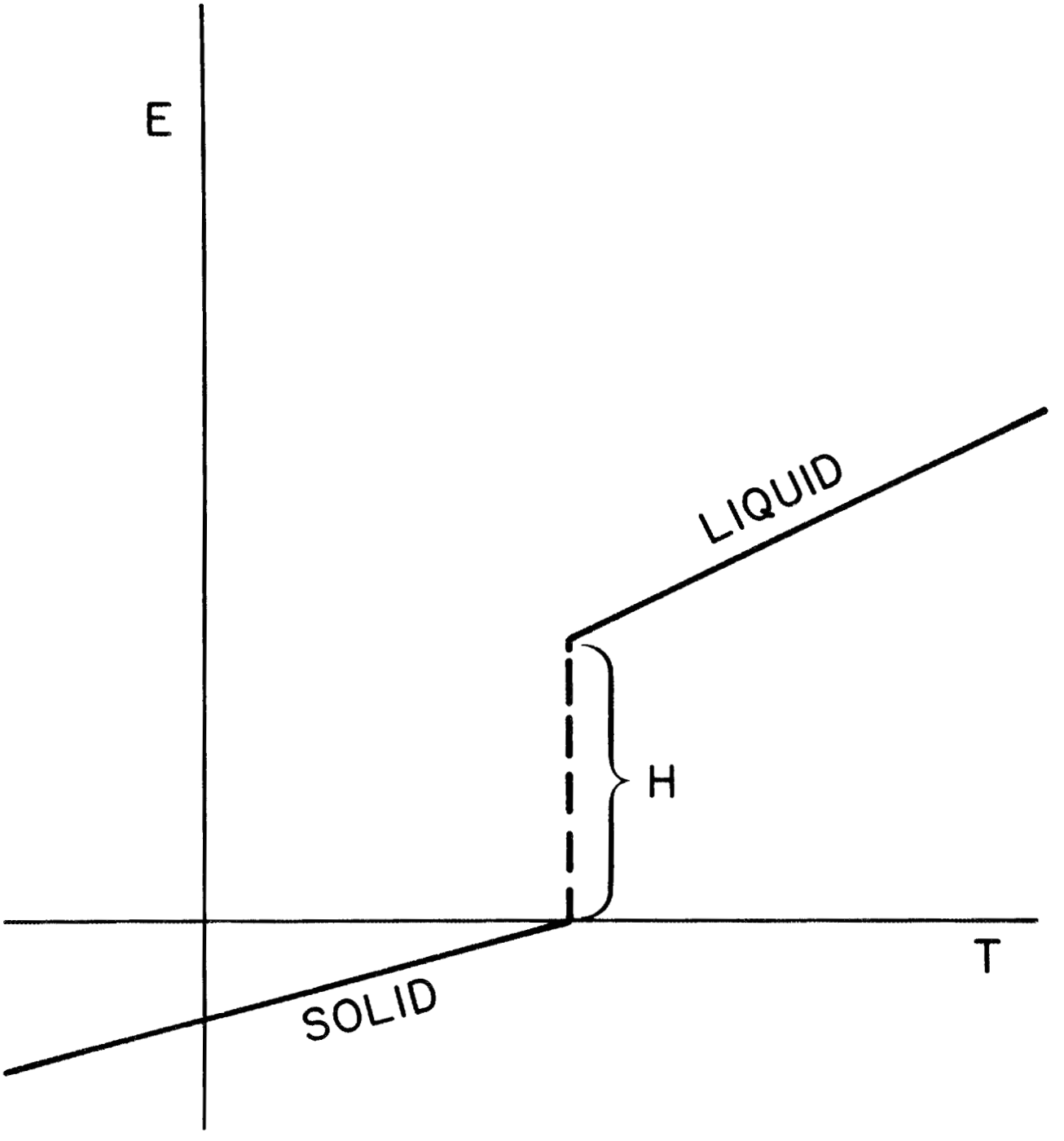

Figure 1. In the simplest case, the enthalpy-temperature relationship is piecewise linear.

and J intervals are the intervals for which the model provides approximations for average enthalpy and temperature values. Denote by L_l the interval $(x_l - \Delta x/2,\ x_l + \Delta x/2)$ for $l = 1, 2, \ldots,\ nx - 1$ and by M_m the interval $(y_m - \Delta y/2,\ y_m + \Delta y/2)$ for $m = 1, 2, \ldots,\ ny - 1$. Denote by L_0 the interval $(0, \Delta x/2)$ and by L_{nx} the interval $(lx - \Delta x/2,\ l_x)$. Similarly, denote by M_0 the interval $(0, \Delta y/2)$ and by M_{ny} the interval $(ly - \Delta y/2,\ ly)$. The L and M intervals are intervals for which the model requires approximate values of the thermal conductivities. Figure 2 shows how the I and L intervals interleave.

$$\begin{array}{ccccccccccccccccc}
\cdot & I_1 & \cdot & I_2 & \cdot & I_3 & \cdot & I_4 & \cdot & I_5 & \cdot & I_6 & \cdot & I_7 & \cdot & I_8 & \cdot & \ldots \\
\hline
L_0 & \cdot & L_1 & \cdot & L_2 & \cdot & L_3 & \cdot & L_4 & \cdot & L_5 & \cdot & L_6 & \cdot & L_7 & \cdot & L_8 & \ldots
\end{array}$$

Figure 2. Interleaved Intervals I_j and L_j for $j = 0, 1, \cdots$.

Because we impose a flux boundary condition on the top of the box and temperature on the bottom, we partition $[0, lz]$ differently. Given a positive integer nz, set $\Delta z = lz/(nz + 1/2)$. Let $z_j = j\,\Delta z$ for $j = 0, 1, 2, \ldots,\ nz$. Denote by K_k the interval $(z_k - \Delta z/2,\ z_k + \Delta z/2)$ for $k = 1, 2, \ldots,\ nz$. Denote by K_0 the interval $(0, \Delta z/2)$. The K intervals are the intervals for which the model provides approximations for average enthalpy and temperature values. Denote by P_p the interval (z_{p-1}, z_p) for $p = 0, 1, 2, \ldots,\ nz$ and by P_{nz+1} the interval $(lz - \Delta z/2,\ lz)$. The P intervals are the intervals for which the model requires approximate values of the thermal conductivities. The domain $[0, lx] \times [0, ly] \times [0, lz]$ is then partitioned by $I_i \times J_j \times K_k$ for $i = 1, 2, \ldots, nx$, $j = 1, 2, \ldots,\ ny$ and $k = 0, 1, 2, \ldots,\ nz$. Nodes are located in the centers of the three dimensional cells defined by $I_i \times J_j \times K_k$ for $i = 1, 2, \ldots,\ nx$, $j = 1, 2, \ldots,\ ny$, and $k = 1, 2, \ldots,\ nz$; and in the centers of the two dimensional cells at the bottom of the parallelepiped defined by $I_i \times J_j \times \{0\}$ for $i = 1, 2, \ldots, nx$ and $j = 1, 2, \ldots, ny$.

We discretize the problem by replacing the time derivative with the standard forward difference quotient and the spatial derivatives by second order centered difference quotients of the form

$$(k(T)T_x)_x \approx \frac{k_{i+\frac{1}{2}}(T_{i+1} - T_i) - k_{i-\frac{1}{2}}(T_i - T_{i-1})}{\Delta x^2}$$

where we take $k_{i\pm\frac{1}{2}}$ to be

$$k_{i\pm\frac{1}{2}} = \frac{k(T_i) + k(T_{i\pm1})}{2} .$$

A discrete analog of (1) is

$$\rho\left(\frac{e_{ijk}^{n+1} - e_{ijk}^{n}}{\Delta t}\right) = \frac{[k_{i+\frac{1}{2},jk}(T_{i+1,jk} - T_{ijk})]^{n+\theta} - [k_{i-\frac{1}{2},jk}(T_{ijk} - T_{i-1,jk})]^{n+\theta}}{\Delta x^2} \tag{2}$$

$$+ \frac{[k_{i,j+\frac{1}{2},k}(T_{i,j+1,k} - T_{ijk})]^{n+\theta} - [k_{i,j-\frac{1}{2},k}(T_{ijk} - T_{i,j-1,k})]^{n+\theta}}{\Delta y^2}$$

$$+ \frac{[k_{ijk+\frac{1}{2}}(T_{ijk+1} - T_{ijk})]^{n+\theta} - [k_{ijk-\frac{1}{2}}(T_{ijk} - T_{ijk-1})]^{n+\theta}}{\Delta z^2} ,$$

where $\theta \in [0,1]$ and

$$F^{n+\theta} \equiv (1-\theta)F^n + \theta F^{n+1} .$$

Expanding (2) using the above relation and rearranging terms yields

$$e_{ijk}^{n+1} = \frac{\theta\Delta t}{\rho\Delta x^2}[k_{i+\frac{1}{2},jk}^{n+1}(T_{i+1,jk}^{n+1} - T_{ijk}^{n+1}) - k_{i-\frac{1}{2},jk}^{n+1}(T_{ijk}^{n+1} - T_{i-1,jk}^{n+1})] \tag{3}$$

$$+ \frac{\theta\Delta t}{\rho\Delta y^2}[k_{i,j+\frac{1}{2},k}^{n+1}(T_{i,j+1,k}^{n+1} - T_{ijk}^{n+1}) - k_{i,j-\frac{1}{2},k}^{n+1}(T_{ijk}^{n+1} - T_{i,j-1,k}^{n+1})]$$

$$+ \frac{\theta\Delta t}{\rho\Delta z^2}[k_{ij,k+\frac{1}{2}}^{n+1}(T_{ij,k+1}^{n+1} - T_{ijk}^{n+1}) - k_{ij,k-\frac{1}{2}}^{n+1}(T_{ijk}^{n+1} - T_{ij,k-1}^{n+1})]$$

$$+ b_{ijk}^{n} .$$

where

$$b_{ijk}^{n} = e_{ijk}^{n} + \frac{(1-\theta)\Delta t}{\rho \Delta x^2}\left[k_{i+\frac{1}{2},jk}^{n}(T_{i+1,jk}^{n} - T_{ijk}^{n}) - k_{i-\frac{1}{2},jk}^{n}(T_{ijk}^{n} - T_{i-1,jk}^{n})\right] \tag{4}$$

$$+ \frac{(1-\theta)\Delta t}{\rho \Delta y^2}\left[k_{i,j+\frac{1}{2},k}^{n}(T_{i,j+1,k}^{n} - T_{ijk}^{n}) - k_{i,j-\frac{1}{2},k}^{n}(T_{ijk}^{n} - T_{i,j-1,k}^{n})\right]$$

$$+ \frac{(1-\theta)\Delta t}{\rho \Delta z^2}\left[k_{ij,k+\frac{1}{2}}^{n}(T_{ij,k+1}^{n} - T_{ijk}^{n}) - k_{ij,k-\frac{1}{2}}^{n}(T_{ijk}^{n} - T_{ij,k-1}^{n})\right].$$

For compactness, define

$$\xi_{ijk}^{n+1} \equiv \frac{\theta \Delta t}{\rho \Delta x^2}\left(k_{i+\frac{1}{2},jk}^{n+1} + k_{i-\frac{1}{2},jk}^{n+1}\right)$$

$$+ \frac{\theta \Delta t}{\rho \Delta y^2}\left(k_{i,j+\frac{1}{2},k}^{n+1} + k_{i,j-\frac{1}{2},k}^{n+1}\right)$$

$$+ \frac{\theta \Delta t}{\rho \Delta z^2}\left(k_{ij,k+\frac{1}{2}}^{n+1} + k_{ij,k-\frac{1}{2}}^{n+1}\right).$$

and

$$\zeta_{ijk}^{n+1} \equiv b_{ijk}^{n} + \frac{\theta \Delta t}{\rho \Delta x^2}\left(k_{i+\frac{1}{2},jk}^{n+1}\, T_{i+1,jk}^{n+1} + k_{i-\frac{1}{2},jk}^{n+1}\, T_{i-1,jk}^{n+1}\right)$$

$$+ \frac{\theta \Delta t}{\rho \Delta y^2}\left(k_{i,j+\frac{1}{2},k}^{n+1}\, T_{i,j+1,k}^{n+1} + k_{i,j-\frac{1}{2},k}^{n+1}\, T_{i,j-1,k}^{n+1}\right)$$

$$+ \frac{\theta \Delta t}{\rho \Delta z^2}\left(k_{ij,k+\frac{1}{2}}^{n+1}\, T_{ij,k+1}^{n+1} + k_{ij,k-\frac{1}{2}}^{n+1}\, T_{ij,k-1}^{n+1}\right).$$

Then, equation (3) can be written as

$$e_{ijk}^{n+1} + \xi_{ijk}^{n+1}\, T_{ijk}^{n+1} = \zeta_{ijk}^{n+1}.$$

4. Numerical Solution

C. M. Elliott and J. R. Ockendon [2] suggest using successive overrelaxation (SOR) to solve simultaneously for T_{ijk}^{n+1} and e_{ijk}^{n+1}. Let τ_{ijk}^{p} denote the pth iterate of T_{ijk}^{n+1} and, again for compactness, define

$$z_{ijk}^{p} = b_{ijk}^{n} + \frac{\theta \Delta t}{\rho \Delta x^2} (k_{i+\frac{1}{2},jk}^{p} \tau_{i+1,jk}^{p} + k_{i-\frac{1}{2},jk}^{p+1} \tau_{i-1,jk}^{p+1})$$
$$+ \frac{\theta \Delta t}{\rho \Delta y^2} (k_{i,j+\frac{1}{2},k}^{p} \tau_{i,j+1,k}^{p} + k_{i,j-\frac{1}{2},k}^{p+1} \tau_{i,j-1,k}^{p+1})$$
$$+ \frac{\theta \Delta t}{\rho \Delta z^2} (k_{ij,k+\frac{1}{2}}^{p} \tau_{ij,k+1}^{p} + k_{ij,k-\frac{1}{2}}^{p+1} \tau_{ij,k-1}^{p+1}) ,$$

and

$$c_{ijk}^{p} = \frac{\theta \Delta t}{\rho \Delta x^2} (k_{i+\frac{1}{2},jk}^{p} + k_{i-\frac{1}{2},jk}^{p+1})$$
$$+ \frac{\theta \Delta t}{\rho \Delta y^2} (k_{i,j+\frac{1}{2},k}^{p} + k_{i,j-\frac{1}{2},k}^{p+1})$$
$$+ \frac{\theta \Delta t}{\rho \Delta z^2} (k_{ij,k+\frac{1}{2}}^{p} + k_{ij,k-\frac{1}{2}}^{p+1}) .$$

Note that for a given node, temperature and thermal conductivity values are lagged one iteration at advanced points, but not at previous points. This constitutes a Gauss-Seidel iteration. Our iterative form of the equation to be solved is

$$e_{ijk}^{p+1} + c_{ijk}^{p} \tau_{ijk}^{p+1} = z_{ijk}^{p} . \tag{5}$$

Starting with an initial approximation to T_{ijk}^{n+1}, τ_{ijk}^{0}, a candidate temperature, $\tilde{\tau}_{ijk}^{p}$ is computed for successive p's from

$$\tilde{\tau}_{ijk}^{p+1} = \begin{cases} \dfrac{c_S T_{cr} + z_{ijk}^{p}}{c_{ijk}^{p} + c_S} & \text{if } z_{ijk}^{p} - c_{ijk}^{p} T_{cr} \leqslant 0 , \\ T_{cr} & \text{if } 0 < z_{ijk}^{p} - c_{ijk}^{p} T_{cr} < H , \\ \dfrac{c_L T_{cr} + z_{ijk}^{p}}{c_{ijk}^{p} + c_L} & \text{if } z_{ijk}^{p} - c_{ijk}^{p} T_{cr} \geqslant H , \end{cases} \tag{6}$$

where c_S and c_L are the heat capacities of the solid and liquid, respectively. This assignment will be explained below.

Another candidate temperature, $\hat{\tau}$, is calculated using SOR from

$$\hat{\tau}_{ijk}^{p+1} = \tau_{ijk}^{p} + \omega (\tilde{\tau}_{ijk}^{p+1} - \tau_{ijk}^{p}) , \tag{7}$$

where $\omega \in (1, 2)$ is the relaxation parameter. A discussion of the optimal choice for ω can be found in [2].

The SOR temperature, $\hat{\tau}_{ijk}^{p+1}$, is chosen if $\hat{\tau}_{ijk}^{p+1}$ and τ_{ijk}^{p} both lie on the same side of T_{cr}; the Gauss-Seidel temperature, $\tilde{\tau}_{ijk}^{p+1}$, is chosen otherwise. Precisely stated

$$\tau_{ijk}^{p+1} = \begin{cases} \tilde{\tau}_{ijk}^{p+1}, & \text{if } (\tau_{ijk}^{p} - T_{cr})(\hat{\tau}_{ijk}^{p+1} - T_{cr}) \leqslant 0, \\ \hat{\tau}_{ijk}^{p+1}, & \text{if } (\tau_{ijk}^{p} - T_{cr})(\hat{\tau}_{ijk}^{p+1} - T_{cr}) > 0. \end{cases}$$

This choice avoids oscillation about T_{cr}. Once the iteration has converged to a sufficient tolerance, after $p = R$ iterations say, $\| \tau^{R} - \tau^{R-1} \|_{\infty}$ is less than ϵ and we set $T_{ijk}^{n+1} = \tau_{ijk}^{R}$ and calculate e_{ijk}^{n+1} using

$$e_{ijk}^{n+1} = z_{ijk}^{R-1} - c_{ijk}^{R-1} T_{ijk}^{n+1}. \tag{8}$$

To explain the assignment of τ_{ijk}^{p+1} in (6), we first define $f(s) \equiv z_{ijk}^{p} - c_{ijk}^{p} s$ and note from (5) that $f(\tau_{ijk}^{p+1})$ will be the $(p+1)$th approximation to the enthalpy. It is easy to show that if $f(T_{cr}) \leqslant 0$, then $f(\tau_{ijk}^{p+1}) \leqslant 0$; if $0 < f(T_{cr}) < H$, then $0 < f(\tau_{ijk}^{p+1}) < H$ and if $f(T_{cr}) \geqslant H$, then $f(\tau_{ijk}^{p+1}) \geqslant H$. Consider the first branch of (6). Since $f(T_{cr}) \leqslant 0$, we have $f(\tau_{ijk}^{p+1}) \leqslant 0$ and the enthalpy/temperature relationship is

$$e_{ijk}^{p+1} = c_S (\tilde{\tau}_{ijk}^{p+1} - T_{cr}).$$

Solving this and (5) for $\tilde{\tau}_{ijk}^{p+1}$ yields

$$\tilde{\tau}_{ijk}^{p+1} = \frac{c_S T_{cr} + z_{ijk}^{p}}{c_{ijk}^{p} + c_S}.$$

The assignments of the second and third branches in (6) can be justified similarly.

5. CRAY X-MP Implementation

The CRAY X-MP carries out identical calculations on long vectors very quickly. Thus, the longest possible vectors should be created. To insure vectorization is not inhibited, interdependencies among vector elements and IF statements within loops must be avoided.

Consecutive numbering of nodes unfolds the three dimensional array into one long vector. This converts an $nx \times ny \times nz$ array into a vector of length $nx\ ny\ nz$. Suppose i, j, and k are the row, column and level indices of the three dimensional array. Then the corresponding index, l say, of the vector is $l \equiv i + (j-1)nx + (k-1)nx\ ny$. Also, given the index l of the vector, i, j, and k are given by

$$k = \text{Integer}\,[l/(nx\ ny)] + 1$$

$$j = \text{Integer}\,[(l-(k-1)nx\ ny)/nx] + 1$$

$$i = l - (k-1)nx\ ny - (j-1)nx\ .$$

In the red/black ordering of nodes, odd numbered nodes are thought of as "red" and even numbered nodes as thought of as "black." We require an odd number of nodes per row and column. Thus all neighbors of a given node are of the opposite color. This ordering eliminates interdependencies among vector elements. In our implementation, red nodes are updated first using black nodal values from the previous time step. Black nodes are then updated using the new red nodal values. In effect, we make two Jacobi-type updates to get one Gauss-Seidel iteration. For a more complete description of red/black ordering and a discussion of its effects on convergence of Gauss-Seidel iterations, see [3].

Setting thermal conductivities, determining boundary nodes and applying boundary conditions, and calculating temperatures from enthalpy values all involve a decision-making process. Since IF statements within loops inhibit vectorization, an alternate technique is required. We create Boolean variables and replace IF statements with expressions involving the Boolean variables. In the following discussion, we make extensive use of the *sign* function defined in [4] by

$$sign(a,b) = \begin{cases} |a|, \text{ if } b \geqslant 0, \\ -|a|, \text{ if } b < 0. \end{cases}$$

We first describe how thermal conductivities are computed and used. We calculate z using

$$z = b(i) + \frac{\theta\,\Delta t}{\rho\,\Delta x^2}\left(k_{right}\,T(i+1) + k_{left}\,T(i-1)\right)$$
$$+ \frac{\theta\,\Delta t}{\rho\,\Delta y^2}\left(k_{back}\,T(i+nx) + k_{front}\,T(i-nx)\right) \tag{9}$$
$$+ \frac{\theta\,\Delta t}{\rho\,\Delta z^2}\left(k_{above}\,T(i+nxny) + k_{below}\,T(i-nxny)\right).$$

and c using

$$c = \frac{\theta\,\Delta t}{\rho\,\Delta x^2}\left(k_{right} + k_{left}\right)$$
$$+ \frac{\theta\,\Delta t}{\rho\,\Delta y^2}\left(k_{back} + k_{front}\right) \tag{10}$$
$$+ \frac{\theta\,\Delta t}{\rho\,\Delta z^2}\left(k_{above} + k_{below}\right).$$

The subscript *right* refers to $i + ½, j, k$ in the three dimensional array; *left* to $i - ½, j, k$; *back* to $i, j + ½, k$; *front* to $i, j - ½, k$; *above* to $i, j, k + ½$; and *below* to $i, j, k - ½$. The thermal conductivities are computed from

$$k_{right} = \begin{cases} k_S \text{ if } T(i) < T_{cr} \text{ and } T(i+1) < T_{cr} \\ k_L \text{ if } T(i) \geqslant T_{cr} \text{ and } T(i+1) \geqslant T_{cr} \\ (k_S + k_L)/2 \text{ otherwise}, \end{cases}$$

$$k_{back} = \begin{cases} k_S \text{ if } T(i) < T_{cr} \text{ and } T(i+nx) < T_{cr} \\ k_L \text{ if } T(i) \geqslant T_{cr} \text{ and } T(i+nx) \geqslant T_{cr} \\ (k_S + k_L)/2 \text{ otherwise}, \end{cases}$$

etc.

To construct k_{right} using Boolean variables, we create

$$lqcntr = 1 - \text{Integer}\,[1.0 - \text{sign}(0.5, T(i) - T_{cr})]\,,$$

and

$$lqrt = 1 - \text{Integer}\,[1.0 - \text{sign}(0.5, T(i+1) - T_{cr})]\,.$$

Then, we define

$$k_{right} \equiv 0.5\,[(lqcntr + lqrt)\,k_L + (2 - lqcntr - lqrt)\,k_S]\,. \tag{11}$$

The results of these calculations are summarized in Table 1.

Table 1

	$T(i) \geqslant T_{cr}$ and $T(i+1) \geqslant T_{cr}$	$T(i) < T_{cr}$ and $T(i+1) < T_{cr}$	$T(i) \geqslant T_{cr}$ and $T(i+1) < T_{cr}$	$T(i) < T_{cr}$ and $T(i+1) \geqslant T_{cr}$
$lqcntr$	1	0	1	0
$lqrt$	1	0	0	1
$lqcntr + lqrt$	2	0	1	1
$2 - (lqcntr + lqrt)$	0	2	1	1
k_{right}	k_L	k_S	$\frac{(k_L + k_S)}{2}$	$\frac{(k_L + k_S)}{2}$

Similarly, for all thermal conductivities in (9) and (10).

Boundary nodes are scattered throughout the vector due to unfolding the three dimensional array. The calculation is modified at these nodes. Consider a right boundary node with zero flux boundary conditions. For this node, the $k^{n+1}_{i+\frac{1}{2},jk}\,(T^{n+1}_{i+1,jk} - T^{n+1}_{ijk})$ term in (3) should be zero and thus the $k_{right}\,T(i+1)$ term in (9) would be zero. This is accomplished by modifying the thermal conductivities so that $k_{right} = 0$ at right boundary nodes, $k_{left} = 0$ at left boundary nodes, etc.

The index of a right boundary node is a multiple of the number of nodes per row. Thus

$$ix = i - \text{Integer}(i/nx)\,nx$$

is zero for a right boundary node. Here i is the running vector index and nx is the number of nodes per row. Then

$$nxrt = \text{Integer}[(ix + nx - 1)/nx]$$

is equivalent to

$$nxrt = \begin{cases} 0 \text{ if } i \text{ is a right boundary node} \\ 1 \text{ otherwise.} \end{cases}$$

The thermal conductivity on the right, k_{right}, is computed as previously explained except that (11) becomes

$$k_{right} = nxrt\ 0.5\,[(lqcntr + lqrt)\,k_L + (2 - lqcntr - lqrt)\,k_S]. \tag{12}$$

Computations of thermal conductivities at other boundaries are similarly modified.

We next explain how to compute the candidate temperature $\tilde{\tau}^{p+1}$ and the new temperature τ^{p+1} using Boolean variables. We wish to compute $\tilde{\tau}^{p+1}$ as in (6). Consider the following definitions.

$m_1 = 1 - \text{Integer}\,(1.0 - \text{sign}\,(0.5,\ c\,T_{cr} - z))$.

$m_2 = 1 - \text{Integer}\,(1.0 - \text{sign}\,(0.5,\ z - c\,T_{cr} - H))$.

$l_1 = (1 - m_1)(1 - m_2)$.

$l_2 = 1 - l_1$.

Values of these Boolean variables as functions of z and c are shown in Table 2. Using these variables, we compute $\tilde{\tau}^{p+1}$ according to

$$\tilde{\tau}^{p+1} = \frac{l_2(m_1 c_S\,T_{cr} + z + m_2(c_L\,T_{cr} - H))}{(c + m_1 c_S + m_2 c_L + l_1\,1.0)} + l_1 T_{cr}$$

The possible results of these computations are presented in Table 2.

Table 2

	$z - c\,T_{cr} \leqslant 0$	$0 < z - c\,T_{cr} < H$	$z - c\,T_{cr} \geqslant H$
m_1	1	0	0
m_2	0	0	1
l_1	0	1	0
l_2	1	0	1
$\tilde{\tau}^{p+1}$	$\dfrac{c_S\,T_{cr} + z}{c + c_S}$	T_{cr}	$\dfrac{c_L\,T_{cr} + z - H}{c + c_L}$

The calculation of $\hat{\tau}^{p+1}$ using (7) is straightforward. Finally, to compute $\tilde{\tau}^{p+1}$ we define another Boolean variable, m_3 by

$$m_3 = 1 - \text{Integer}\{1.0 - \text{sign}[0.5, (T_{cr} - T(i))(\hat{\tau}^{p+1} - T_{cr})]\},$$

and calculate τ^{p+1} using

$$\tau^{p+1} = m_3\tilde{\tau}^{p+1} + (1 - m_3)\hat{\tau}^{p+1}. \tag{13}$$

To summarize, enthalpy and temperature at each node are updated as follows.

1. Compute $b(i)$ for each node using Equation (4).
2. Set $\tau^0(i) = T^n(i)$.
3. Set $p = 0$.

For each node

4. Compute k_{right}, k_{left}, k_{back}, k_{front}, k_{above}, and k_{below}, using Equation (12) and similar equations.
5. Compute z using (9).
6. Compute c using (10).
7. Compute $\tau^{p+1}(i)$ using (13).

Then,

8. Compute $tmaxdif \equiv \max\limits_{1 \leqslant i \leqslant n} |\tau^p(i) - \tau^{p+1}(i)|$.

If $tmaxdif > \epsilon$

Set $p = p+1$.

Go to Step 4.

Otherwise,

Set $T^{n+1}(i) = \tau^{p+1}(i)$.

Compute $e^{n+1}(i)$ using (8).

"Red" nodes are updated first and then black nodes. Boundary nodes are not treated differently from interior nodes. The boundary conditions are handled by setting the appropriate thermal conductivities to zero as previously described.

6. Test Results

A CFT FORTRAN code was developed to implement the algorithm described in section 4 using the techniques outlined in section 5. We present results for the following test problems:

Box Dimensions: 1.2 m × 1.0 m × 0.8 m.

Initial Conditions: $T_0 = 0\,°C$ $H_0 =$ 0.2, 8.0, 20.0, and 200.0 kJ/kg.

Boundary Conditions: flux = 0 kJ/m^2-s on walls and top,

$T(x,y) = -10 - 3x - 4y^2$ on the bottom.

Physical Constants: Critical Temperature: $T_{cr} = 0\,°C$.

Thermal Conductivity

of solid: $k_S = 1.0 \times 10^{-3}$ kJ/m-s-°C

of liquid: $k_L = 1.0 \times 10^{-2}$ kJ/m-s-°C

Specific Heat: $c_S = c_L = 1.0$ kJ/kg-°C

Density: $\rho = 1.0$ kg/m^3

Latent Heat: H = 0.2, 8.0, 20.0, 200.0 kJ/kg

These data do not represent any real material but were used only to verify the program.

At all points on the bottom of the box the imposed temperature is well below T_{cr}. This causes all material on the box bottom to solidify initially. One expects the interface surface to be flat at small times. Since the temperature distribution is not uniform, solidification proceeds at non-uniform rates. The back right corner, where T = -17 °C, solidifies more quickly than the front left corner where T = -10 °C. At intermediate times one expects a solid/liquid interface to develop that resembles the temperature distribution on the bottom. However heat is diffusing laterally as well as upward. This allows a lateral equilibrium to be established over long time intervals. Thus one expects the interface surfaces to again be flat at large times.

In Figures 3-6, we have plotted the solid/liquid interface when it reaches the middle of the box for various values of the latent heat, H. These are interface surfaces in the sense that all material below the surface has solidified and all material on or above the surface is liquid or mush. When the latent heat is small as in figure 3, the process moves very quickly. An interface surface that resembles the temperature distribution never really develops. In figures 4, 5, and 6, we see the interface surface as it starts to develop. The back right is solidifying more rapidly than the left front. Also notice the time when the surface reaches the middle of the box. It takes almost 100 times longer for the solid/liquid interface to reach this point when H = 200 kJ/kg than it does when H = 0.2 kJ/kg.

In these experiments, the number of nodes in the x-direction is 7, in y-direction is 5 and in z-direction is 15. We have taken $\theta = ½$, $\omega = 1$, $\epsilon = 10^{-4}$, and Δt = explicit timestep size = 0.089 sec. The coarsness of the plotting grid creates what appear to be edges and corners in the plotted surfaces. These are artifacts of the plotting and not of the numerical scheme. As the mesh is refined and more points are added to the plotting grid, the interface surfaces become smoother. However, these plots become cluttered and "busy." If the mesh on which computations are performed is refined but the same plotting grid is used, the appearance of the interface surfaces is unchanged.

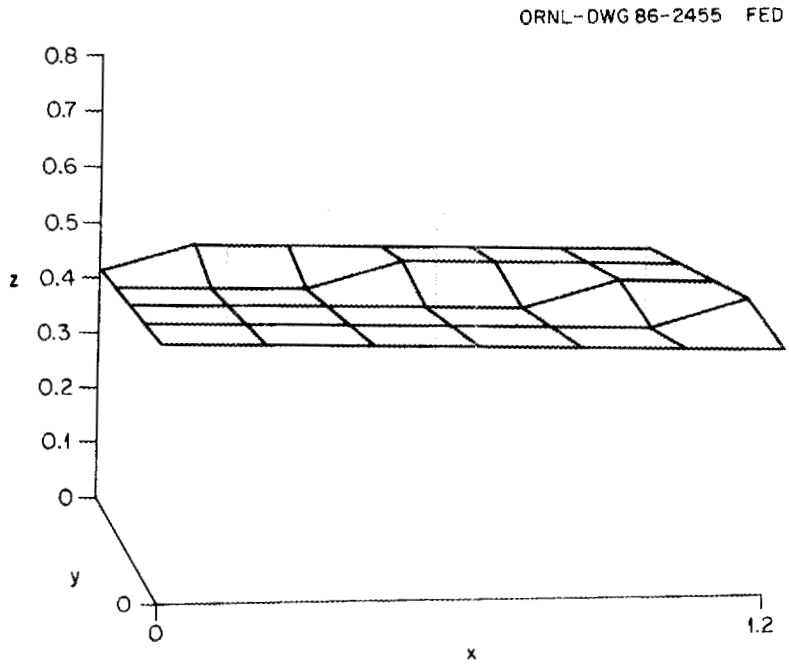

Figure 3. Interface surface when H = 0.2 kJ/kg, t = 1.60 sec.

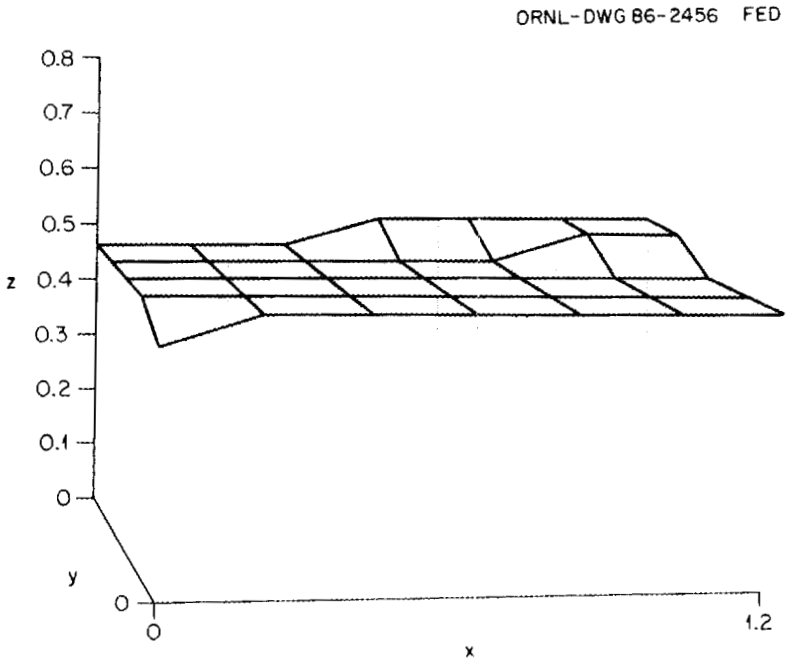

Figure 4. Interface surface when H = 8.0 kJ/kg, t = 11.37 sec.

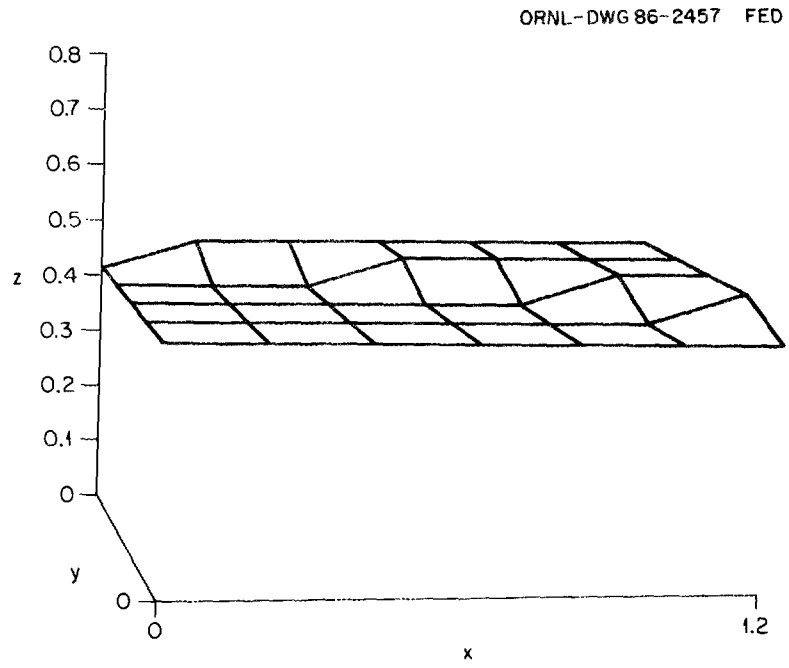

Figure 5. Interface surface when H = 20.0 kJ/kg, t = 19.89 sec.

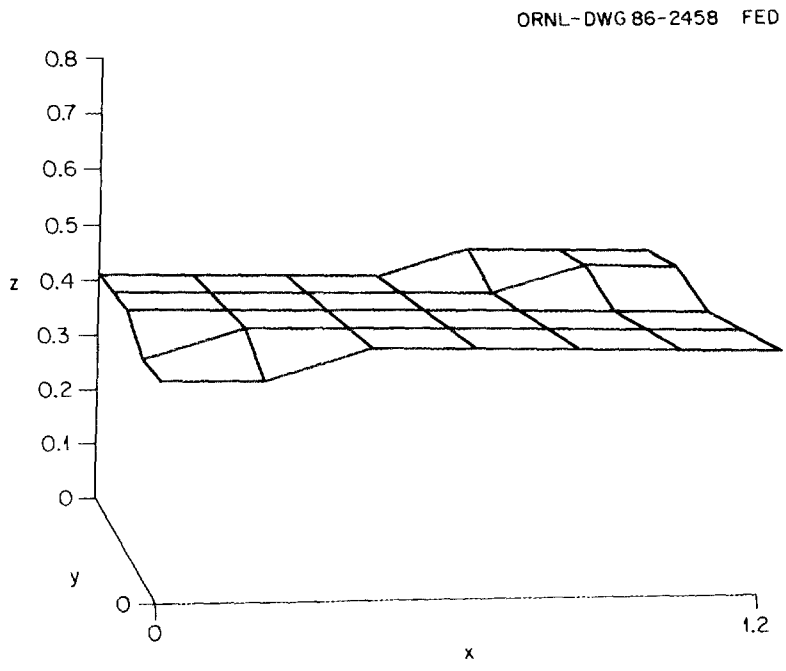

Figure 6. Interface surface when H = 200.0 kJ/kg, t = 159.12 sec.

References

[1] Crank, J., *Free and Moving Boundary Problems*, Oxford University Press, New York (1984).

[2] Elliot, C. M. and J. R. Ockendon, *Weak and Variational Methods for Moving Boundary Problems*, Pitman, Boston (1982).

[3] Hageman, L. A. and D. M. Young, *Applied Iterative Methods*, Academic Press, New York (1981).

[4] Cray Research, Inc., *CRAY-1 and CRAY X-MP Computer Systems FORTRAN (CFT) Reference Manual*, Publication Number SR-0009, Cray Research, Inc. (1983).

ORNL/TM-10034

INTERNAL DISTRIBUTION

1. L. S. Abbott
2. P. S. Damiano
3. M. V. Denson
4. J. B. Drake
5. G. A. Geist
6. L. J. Gray
7-8. R. F. Harbison
Mathematical Sciences Library
9. M. T. Heath
10. A. K. Hudson
11. W. E. Lever
12. F. C. Maienschein
13. M. D. Morris
14. E. Ng
15. S. Thompson
16. R. C. Ward
17-21. M. A. Williams
22-26. D. G. Wilson
27. A. Zucker
28. P. W. Dickson, Jr. (Consultant)
29. G. H. Golub (Consultant)
30. R. M. Haralick (Consultant)
31. D. Steiner (Consultant)
32. Central Research Library
33. K-25 Plant Library
34. ORNL Patent Office
35. Y-12 Technical Library
Document Reference Section
36. Laboratory Records - RC
37-38. Laboratory Records Department

EXTERNAL DISTRIBUTION

39. Dr. Donald M. Austin, Division of Engineering, Mathematical and Geo-Sciences, Office of Basic Energy Sciences, Germantown Building, J-311, Department of Energy, Washington, DC 20545

40. Professor John Bruch, Department of Mechanical and Environmental Engineering, University of California at Santa Barbara, Santa Barbara, CA 93106

41. Dr. James S. Coleman, Division of Engineering, Mathematical and Geo-Sciences, Office of Basic Energy Sciences, Department of Energy, ER-17, MC G-256, Germantown, Washington, DC 20545

42. Dr. Sam Coriell, U. S. National Bureau of Standards, Mathematical Analysis Section, Washington, DC 20234

43. Dr. James Corones, Ames Laboratory, Iowa State University, Ames, IA 50011

44. Professor Robert E. Funderlic, Computer Sciences Department, North Carolina State University, Raleigh, NC 27650

45. Professor Eugene Isaacson, New York University, Courant Institute of Mathematical Sciences, 251 Mercer Street, New York, NY 10012

46. Dr. William R. King, Manager, ASW Software, Martin Marietta Aerospace, Baltimore Division MP 405, 103 Chesapeake Park Plaza, Baltimore, Maryland 21220

47. Professor Peter D. Lax, Courant Institute of Mathematical Sciences, New York University, 251 Mercer Street, New York, NY 10012

48. Dr. Alex Lehoczky, ES72 Space Science Laboratory, Marshall Space Flight Center, Huntsville, AL 35812

49. G. T. McAllister, Department of Mathematics, Christmas-Saucon Hall #14, Lehigh University, Bethlehem, PA 18015

50. G. E. McCluskey, Jr., Department of Mathematics, Christmas-Saucon Hall #14, Lehigh University, Bethlehem, PA 18015

51. Dr. Basil Nichols, T-7, Mathematical Modeling and Analysis, Los Alamos Scientific Laboratory, P. O. Box 1663, Los Alamos, NM 87545

52. Major C. E. Oliver, Division of Engineering, Mathematical and Geosciences, Office of Basic Energy Sciences, U. S. Department of Energy, ER-15, Room G-350, Germantown Building, Washington, DC 20545

53. E. P. Salathe, Department of Mathematics, Christmas-Saucon Hall #14, Lehigh University, Bethlehem, PA 18015

54. M. Schechter, Department of Mathematics, Christmas-Saucon Hall #14, Lehigh University, Bethlehem, PA 18015

55. Professor Subrata Sengupta, Department of Mechanical Engineering, University of Miami at Coral Gables, Coral Gables, FL 33124

56. Dr. Robert Siegel, Head, Analytical Fluid Mechanics Section, NASA Lewis Research Center, Cleveland, OH 44135

57. Dr. Frank Szofran, ES72 Space Science Laboratory, Marshall Space Flight Center, Huntsville, AL 35812

58. Office of Assistant Manager for Energy Research and Development, U.S. Department of Energy, Oak Ridge Operations Office, Oak Ridge, TN 37830

59-86. Technical Information Center.